ELSEVIER

Chemical Engineering Journal 85 (2002) 119–126

Chemical Engineering Journal

www.elsevier.com/locate/cej

Local mass-transfer distribution in the channels of a serpentine flow baffled parallel plate cell

C.F. Oduoza, A.A. Wragg*

Department of Engineering, University of Exeter, Harrison Engineering Building, North Park Road, Exeter, Devon EX4 4QF, UK

Received 12 December 2000; accepted 23 July 2001

Abstract

Mass-transfer measurements were made in a parallel plate cell equipped with baffles which produced a three-channel serpentine flow pattern and three-dimensional mass-transfer distribution effects. The entry and exit configurations were in the form of slots of rectangular cross-section. Local mass-transfer coefficient values obtained in the different channels, using surface-flush microelectrodes, reflected the complex hydrodynamics associated with phenomena such as the cell inlet and exit effects, the flow reversal effects at the baffles and preferential flow phenomena in the channels. Mass-transfer measurements obtained by averaging point measurements over various zones of the cell compared favourably with those of other workers. A hydrodynamic model of flow in the cell corresponded well to the measured mass-transfer distribution.

Keywords: Parallel plate cell; Mass transfer; Hydrodynamics; Baffles; Electrochemical flow cell

1. Introduction

The parallel plate cell is the most commonly used of all commercial electrochemical reactors in view of its simplicity of design, construction and operation and also its favourable primary current and potential distribution properties. However, interesting tertiary current distribution phenomena due to mass-transfer effects may be encountered resulting from complex combinations of geometry and hydrodynamics, especially in entry and exit regions. High mass-transfer rates at low volumetric flow rates can be achieved by using a baffle system which creates a serpentine flow path in the cell. Goodridge et al. [1] studied mass transfer in different sizes of baffled cells using the electrochemical limiting current measurement method. One of their cells had similar dimensions to that used in this work. Wragg and Leontaritis [2] described measurements of local mass-transfer and current distributions in a parallel plate cell, of similar dimensions to one of the Goodridge and Mamoor cells, in both a baffled and an unbaffled configuration. They demonstrated an overall superior average performance of the baffled cell as compared to that of the unbaffled cell. Wragg et al. [3] studied mass-transfer distributions near cell entries and corners in electrochemical flow cells, while Bengoa et al. [4] carried out flow visualisation studies and modelling of a filter-press type electrochemical reactor. More recently, Oduoza and Wragg [5] also studied the effects of baffle length on mass transfer in a parallel plate rectangular electrochemical cell again showing the mass transfer enhancing effect of the baffled configuration compared to the unbaffled. They also showed that the longer the baffle length, the higher is the mass transfer.

Rectangular cross-sectioned channels with sharp 180° turns are also often utilised for the passage of fluids in various types of thermal equipment. The flow field in such channels has a three-dimensional structure, due to the additive effects of the secondary flow induced by the centrifugal force in flowing around the turn, and the flow separation caused by the abrupt change in the flow direction in the turn. Therefore, under forced convection heat transfer, the local heat-transfer rates are expected to change in a complex manner. Since steep variations in the local heat transfer increase thermal stresses and affect the lifetime of components, detailed data on local heat transfer in such channels are important to the design of components used under severe thermal conditions. One of the typical applications is found in the internal cooling passages of gas turbine components exposed to high temperature gas flow [6–11]. Heat/mass-transfer characteristics for turbulent flow in rectangular cross-sectioned two-pass channels with a sharp 180° turn have been examined by Hirota et al. [11] using the naphthalene sublimation method. This work relates strongly to the serpentine flow produced in the present cell.

* Corresponding author. Tel.: +1392-263656; fax: +1392-217965.
E-mail address: a.a.wragg@ex.ac.uk (A.A. Wragg).

1385-8947/02/$ – see front matter
PII: S1385-8947(01)00215-7

Nomenclature

A	electrode surface area (m^2)
c_∞	bulk concentration of reacting species (mol/m^3)
d_e	equivalent diameter of channel (m) (defined as 4 × cross-sectional flow area/wetted perimeter for either the whole cell or an individual channel as appropriate)
D	diffusion coefficient (m^2/s)
F	Faraday constant (96487 C/mol)
I_L	limiting electrolysis current (A)
K_X, K_L	local and zone-mean mass-transfer coefficients, respectively (m/s)
L	dimension of an electrode segment or zone (m)
u	mean fluid velocity in a channel (m/s)
x	distance along channel (m)
z	Number of electrons exchanged in electrode reaction

Dimensionless groups

Re	Reynolds number ($d_e u\rho/\mu$)
Sc	Schmidt number (ν/D)
Sh_{de}	Sherwood number based on duct equivalent diameter ($K_L d_e/D$)

Greek letters

μ	dynamic viscosity of fluid (kg/s m)
ν	kinematic viscosity of fluid (m^2/s)
ρ	fluid density (kg/m^3)

This work describes the effects of entrance and exit configurations as well as baffle design on local mass transfer in a rectangular parallel plate cell. The basic differences between the cell design here and those used in the previous work [1,2] lies in the entry and exit configurations and in the design of the baffles. The present design produced a simpler geometry to facilitate a parallel programme of numerical modelling in the context of a collaborative project [12]. There is, therefore, a difference in the hydrodynamics and pressure drop in the two systems and, consequently, in the mass-transfer behaviour.

2. Experimental

2.1. Cell manufacture and electrode assembly

The cell consisted of two parallel 3 mm thick plain nickel plate electrodes of surface dimensions 150 mm × 150 mm, separated by an inter-electrode distance of 10 mm. The electrodes were glued into PVC backing plates so that just one face of each electrode was active. The cell was oriented horizontally with the cathode plate facing upwards. The two electrode plates were separated by means of a PVC frame which also held the two baffles and into which the entry and exit flow slots were cut. Fig. 1 shows a plan view of the cathode plate showing how the baffles divide the flow into three parallel channels. The flow entered and exited via 32 mm × 7.2 mm slots machined through the frame as also shown in Fig. 1. The PVC baffles occupied the full 10 mm interelectrode gap and were 125 mm in length and of thickness 5 mm; thus each of the three channels defined by the baffles was nominally 46.7 mm wide.

Three different cathode plates were constructed so that local mass-transfer measurements could be made in a total of nine different zones of the cell. Six by six arrays of 1 mm diameter surface-flush nickel wire electrodes were incorporated into three different cathode plates at distinct locations, i.e. in the corner, flank and central zones, as shown in Fig. 2. The microcathodes were glued into 1.20 mm diameter holes using Araldite 2004. By assembling the cell with the corner and flank instrumented zones rotated progressively by 90° for each series of experiments, the entire surface of the cathode of the cell could be monitored for observation of local mass-transfer behaviour. A total of 9 × 36, i.e. 324 microcathode measuring positions was achieved, thus providing very detailed mapping of the local limiting current density and local mass-transfer distribution.

It is important to point out that this work employs square-cut PVC baffles, whereas those of Goodridge et al. [1] and Wragg and Leontaritis [2] were full length with lozenge-shaped openings. Again, while the entry and exit slots into the present cell were rectangular shaped (32 mm × 7.2 mm), those of the previous workers [1,2] were three holes each 5 mm in diameter. These geometric differences are crucial to the ensuing hydrodynamic and mass-transfer behaviour. Readers may find the three-dimensional perspective of the reactor shown as Fig. 2 of [2] to be helpful in appreciating the cell geometry.

2.2. Flow rig

The rig carrying the cell consisted of a 100 dm^3 reservoir, equipped with a cooling coil, a Beresford PV 121 chemical pump and rotameters for flow measurement. The cell was mounted horizontally, and made in grey PVC to provide light proofing for compatibility with use of the ferri-ferrocyanide electrolyte with sodium hydroxide electrolyte. The flow rig was equipped with several drains and an emergency dump tank. Oxygen-free nitrogen was bubbled through the electrolyte for several hours prior to experiments to remove dissolved oxygen; a nitrogen blanket was also maintained above the electrolyte during runs. It was possible to regulate the temperature in the reservoir by means of heat exchangers supplied with a mixture of cold and hot tap water.

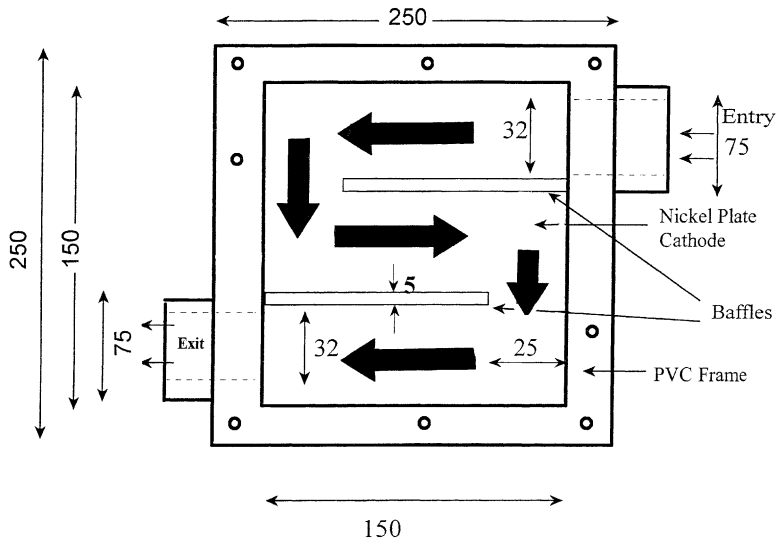

Fig. 1. Plan view of cathode showing frame and plate (dimensions in millimetre).

2.3. Electrolyte

The electrolyte was an aqueous solution of 0.005 M potassium ferricyanide, 0.01 M potassium ferrocyanide and 0.5 M sodium hydroxide ($K_3Fe(CN)_6/K_4Fe(CN)_6/NaOH/H_2O$). The ferrocyanide concentration was double the ferricyanide concentration to ensure a limiting mass-transfer rate at the cathode. The electrolyte was prepared using distilled water and Analar grade reagents. Fifty cubic decimetres of solution were prepared for each run. The physical properties of the electrolyte at 20 °C are shown in Table 1.

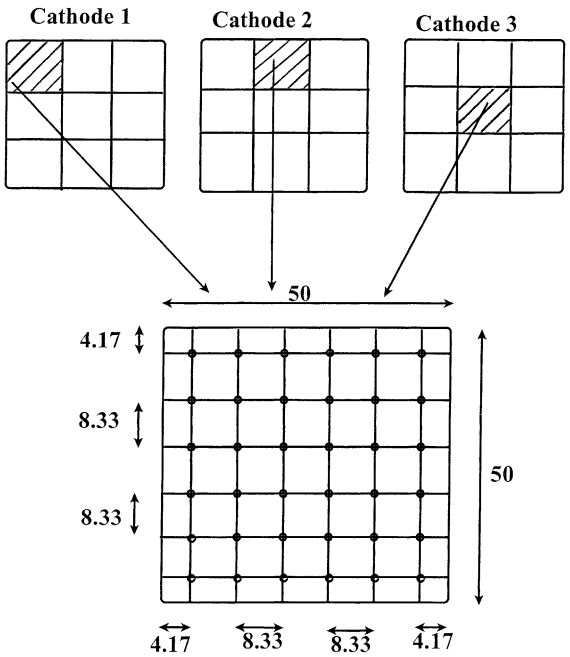

Fig. 2. Diagram showing the three cathodes and the positions of the microelectrode arrays (dimensions in millimetre).

Table 1
Physical properties of the electrolyte at 20 °C

Density (kg/m^3)	1020.5
Viscosity (kg/ms)	1.105×10^{-3}
Diffusivity of ferricyanide ion (m^2/s)	6.631×10^{-10}
Schmidt number	1633

The ferricyanide component of the electrolyte tends to decompose slowly in the presence of light to hydrogen cyanide which both poisons the electrode and alters the concentration. Solution analysis was, therefore, carried out frequently to determine the ferricyanide ion concentration by UV spectrophotometry at a wavelength of absorption 419 nm. The reactions are

$$Fe(CN)_6^{3-} + e \rightarrow Fe(CN)_6^{4-} \quad \text{at the cathode}$$

$$Fe(CN)_6^{4-} \rightarrow Fe(CN)_6^{3-} + e \quad \text{at the anode}$$

2.4. Operation of the flow cell

Electrolyte from the reservoir was pumped via a flow meter to the cell, and then back to the reservoir. There was a provision for by-pass flow to the reservoir, thus facilitating control of electrolyte flow to the cell.

Local mass-transfer coefficients were determined from current–voltage curves with both the macrocathode and the microcathode simultaneously active using an in-house built data-acquisition system. The current–voltage curves for the microcathodes displayed very well-defined limiting currents from which, using the equation

$$K_X = \frac{I_L}{zFAc_\infty}$$

the local mass-transfer coefficients, K_X, were calculated. Measurements were made for a wide variety of volumetric

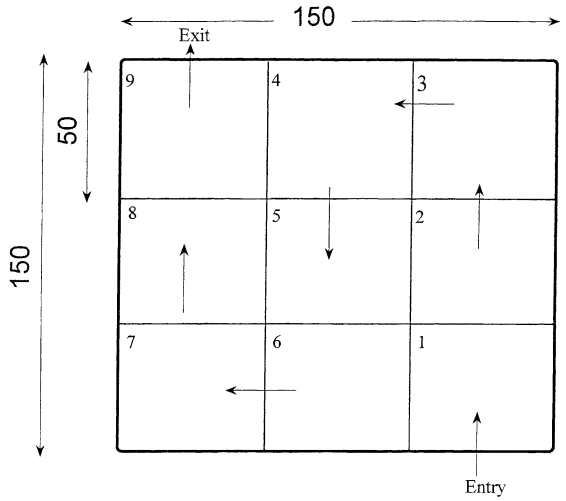

Fig. 3. Key to cathode segments (dimensions in millimetre).

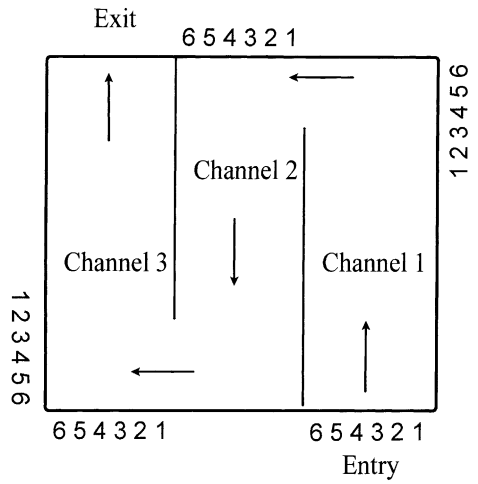

Fig. 4. Key to numbering of flow paths.

flow rates between 5 and 220 dm^3/min. Mass-transfer measurements were made both with the cell in the baffled and baffle-free configuration.

For subsequent discussion of results, the nine zones (or segments) in which the arrays of microelectrodes could be positioned are shown in Fig. 3. Thus segment 1 lies immediately downstream of the cell entry and segment 9 is near the cell exit. Fig. 4 is a key to the numbering of the so-called "flow paths". Thus flow path 1 in channel 1 represents the line of microcathodes at the right-hand side of the first flow channel.

3. Results

Fig. 5 shows the plot of local mass-transfer coefficient distribution for three flow paths (18 measuring points each) in the first channel at $Re = 8780$. High levels of mass-transfer coefficient are evident at the entrance to the cell as a consequence of the inlet jet and there is a gradual decrease as flow development occurs. An increase then occurs towards the first baffle opening. The decrease in mass transfer observed in channel 1 is a result of mass-transfer boundary layer development downstream of the entrance. Flow path 6 experiences the highest mass transfer as the channel end and the baffle opening is approached: reference to Fig. 13 shows the much higher hydrodynamic activity at the left side of the channel in this region. The results for flow between channels 1 and 2 (12 measuring points) are shown in Fig. 6. There is a disturbance to flow as it proceeds through the baffle opening into channel 2 resulting in an increase in mass transfer on all flow paths especially for flow paths 5 and 6 which are closer to the cell end wall. The effect of flow impingement on the second baffle wall in channel 2 produces a further increase in mass transfer.

Fig. 7 shows the mass-transfer distribution for three flow paths in the second (middle) channel. Similarly to channel

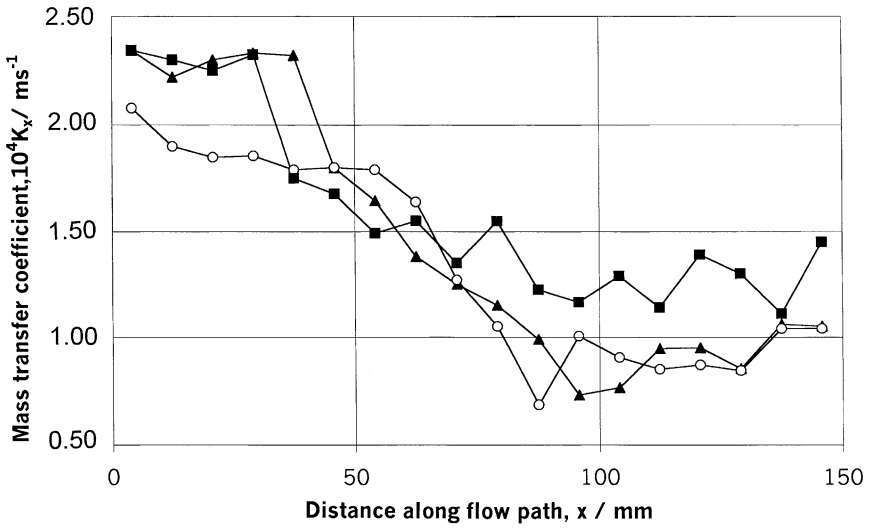

Fig. 5. Plot of local mass-transfer coefficient distribution for three flow paths in channel 1 ($Re = 8780$): (▲) flow path 1; (○) flow path 3; (■) flow path 6.

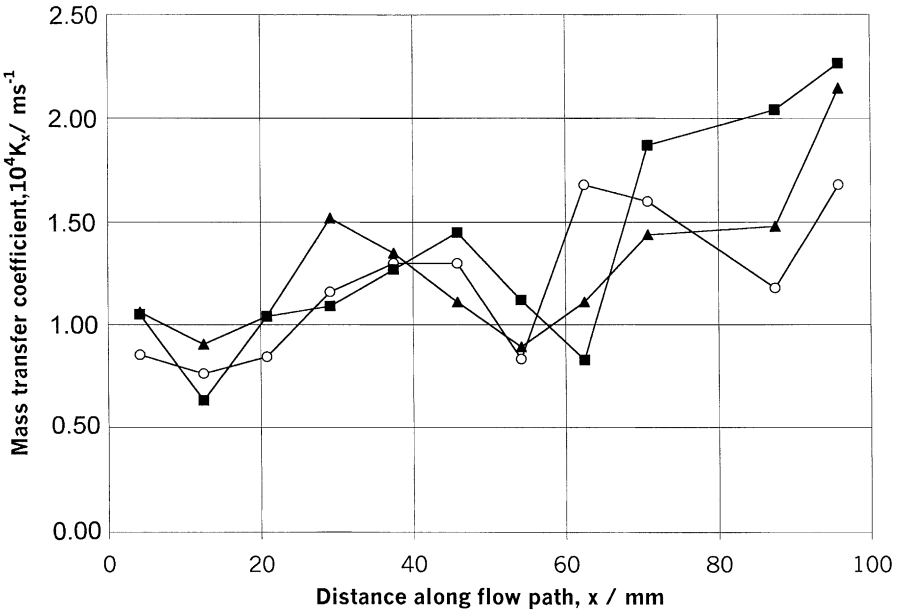

Fig. 6. Plot of local mass-transfer coefficient distribution for three flow paths between channels 1 and 2 ($Re = 8780$): (○) flow path 4; (▲) flow path 5; (■) flow path 6.

1 there is gradual mass-transfer decay as flow progresses downstream due to hydrodynamic development. However, K_X values for flow path 6 are distinctly higher than those for flow paths 3 and 1 due to preferential fluid flow on the right side of the channel (in the flow direction). Towards the middle of the channel there is a relatively flat profile for all flow paths; however, mass transfer in flow path 6 continues to be dominant over the others. Towards the end of channel 2, a further increase in mass transfer is observed especially near the second baffle opening. Fig. 8 shows the mass-transfer distribution for the three flow paths between channels 2 and 3. There is a noticeable increase in mass transfer especially along flow paths 5 and 6, more pronounced on flow path 6. Larger values are obtained as flow impinges on the wall opposite the second baffle opening into channel 3. For the third channel, a decrease in mass transfer again occurs for all flow paths but values along flow path 6 remain high again due to preferential flow on the left side of the channel (Fig. 9). As flow approaches the exit of the cell, a notable increase in K_X is again observed due to flow disturbance in the vicinity of the exit.

Figs. 10 and 11 show the plot of $Sh_{de}Sc^{-0.33}$ against segment numbers (see Fig. 3) for two different Reynolds numbers. These results give values of zone-averaged mass transfer obtained by taking the mean of point measurements over each segment or zone. There is a comparatively higher

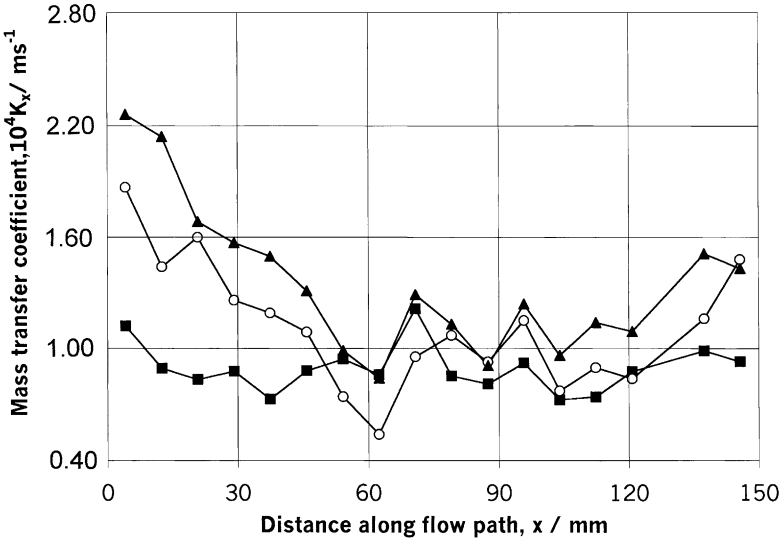

Fig. 7. Plot of local mass-transfer coefficient distribution for three flow paths in channel 2 ($Re = 8780$): (■) flow path 1; (○) flow path 3; (▲) flow path 6.

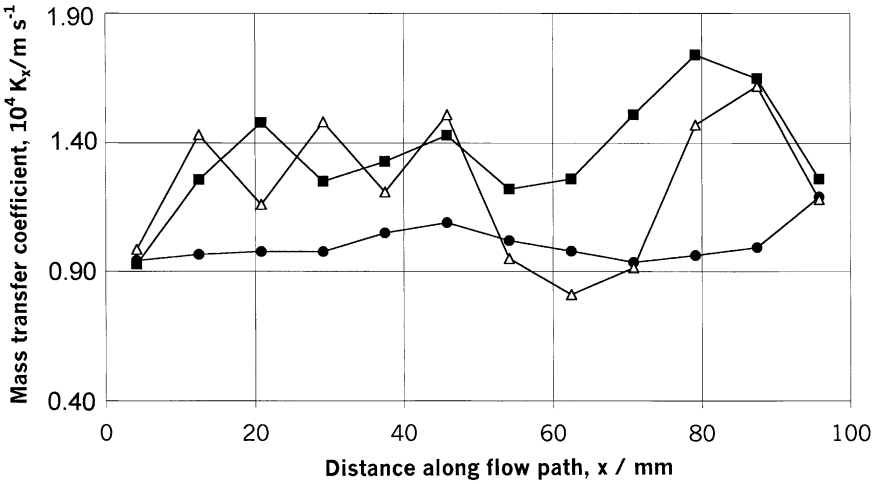

Fig. 8. Plot of local mass-transfer coefficient distribution for three flow paths between channels 2 and 3 ($Re = 8780$): (●) flow path 4; (△) flow path 5; (■) flow path 6.

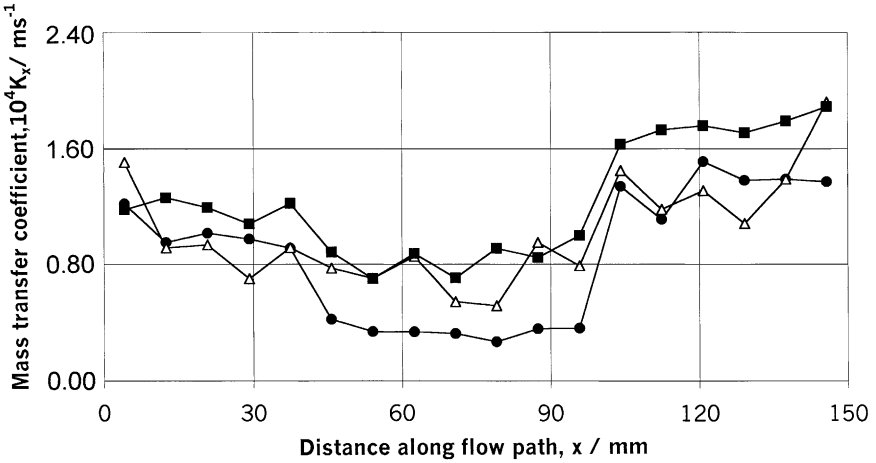

Fig. 9. Plot of local mass-transfer coefficient distribution for three flow paths in channel 3 ($Re = 8780$): (●) flow path 1; (△) flow path 3; (■) flow path 6.

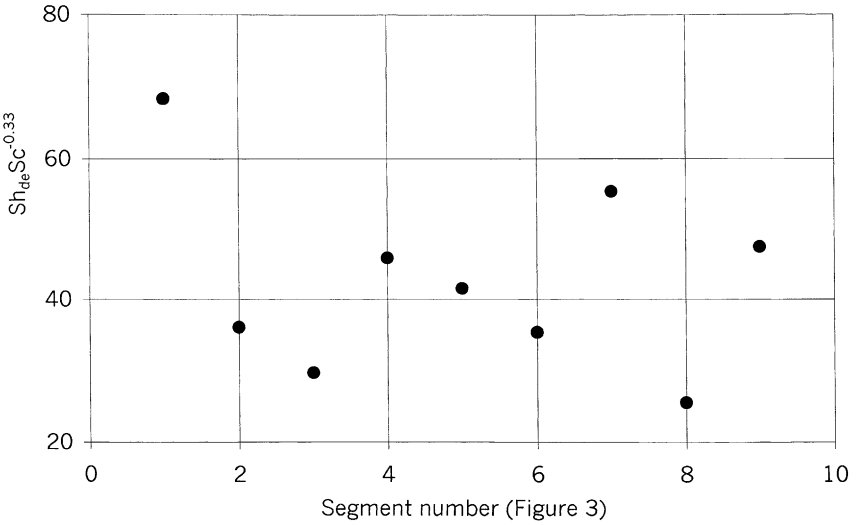

Fig. 10. Plot of $Sh_{de}Sc^{-0.33}$ against segment number at $Re = 250$.

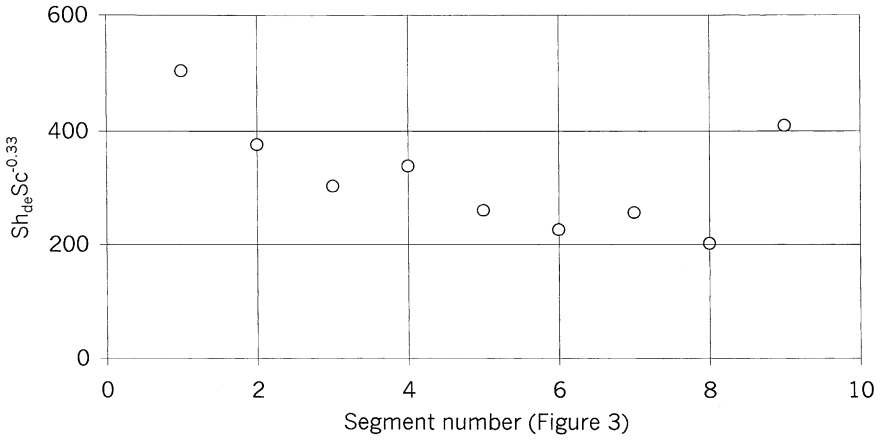

Fig. 11. Plot of $Sh_{de}Sc^{-0.33}$ against segment number at $Re = 8780$.

jump in average Sherwood number from segments 3–4 and from segments 6–7 at the low flow rate compared to the high flow rate. This is due to the flow disturbances in the vicinity of the baffle openings having less relative effect at the higher turbulence levels associated with the higher Reynolds number.

Fig. 12 shows a comparison of the segment by segment measurements with those of Goodridge et al. [1] and Wragg and Leontaritis [2]. Higher mass-transfer values obtained in this work, compared to those in the previous work at a similar Reynolds number, reflect the effect of the present cell geometry. The completely open flow area at the end of the present square-cut baffles contrasts with the lozenge-shaped openings of the previous work and leads to greater accessibility of electrode surface to fast flowing fluid thus enhancing the mass-transfer rate. The new design of the inlet and outlet channels in the form of slots, rather than three separate jets may also have a marginal beneficial effect.

A limited amount of computational fluid dynamic (CFD) modelling of the cell, performed by colleagues at the von Karman Institute of Fluid Mechanics, Brussels [13], gave some insight into the flow patterns occurring and highlighted the regions of intense mass transfer in the neighbourhood of inlets and outlets and also in the regions where the flow changes direction and passes through the baffle openings. Fig. 13 shows a result from a hydrodynamic model of flow in the baffled cell at a Reynolds number of 4736 based on the hydraulic diameter of the inlet duct. We can observe intense hydrodynamic activity at the entrance to the cell, at the baffle openings and at the exit to the cell. The preferential flow adjacent to the right-hand wall of channel 2 and to a lesser extent in channel 3 is also evident. Reverse flow in all channels, and especially channel 1, is also a clear feature.

Comparison with the naphthalene sublimation data of Hirota et al. [11] for a channel with a sharp 180° turn is instructive here and there are some notable similarities between the

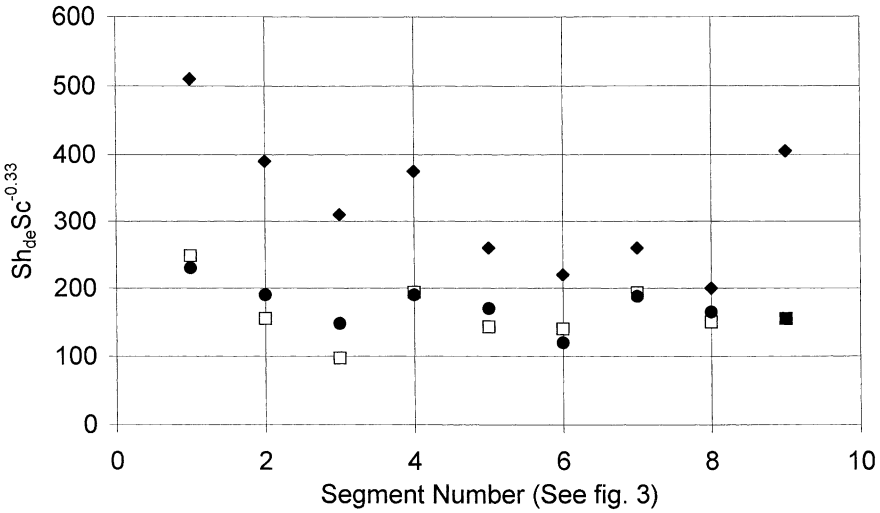

Fig. 12. Plot of $Sh_{de}Sc^{-0.33}$ against segment number at $Re = 8000$: (◆) current work; (●) Goodridge et al.; (□) Wragg and Leontaritis.

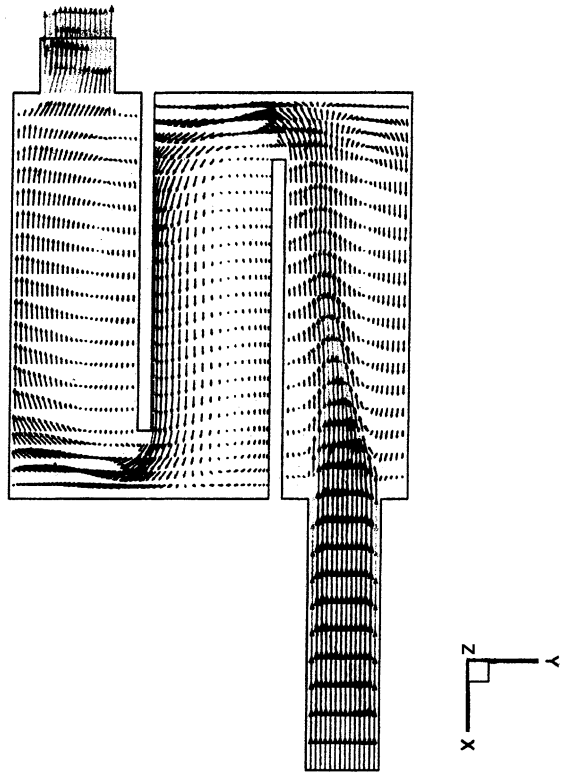

Fig. 13. Plot of flow pattern predictions for the cell (Inlet duct $Re = 4700$).

two sets of work. It is worth mentioning that, via the use of heat- and mass-transfer analogy principles both the electrochemical method used here and the naphthalene sublimation technique are highly useful methods of cold modelling of heat transfer. Hirota et al. [11] used blocks of naphthalene as both the two side walls and the bottom surface of their channels. Fig. 9 of [11] shows how the turn into channel 2 causes enhancement of mean channel mass-transfer rate at four separate Reynolds numbers. Fig. 12(a) of [11], i.e. for the bottom wall, shows a very similar decay in mass transfer along the first channel as in this work, followed by a large enhancement at the turn and into the return channel (channel 2). Fig. 14 of [11] shows local mass-transfer distributions obtained from the naphthalene erosion profiles and the strikingly high values at the end of channel 1 and on the right-hand side of channel 2 indicate very similar behaviour to that in the present work. A full comparison with the results of the naphthalene technique could be made by installing microelectrodes in the vertical side walls and baffles of the present cell. This constitutes a direction for further work.

4. Conclusions

This work demonstrates the effects of entry and exit configurations and of baffles on hydrodynamics in a rectangular parallel plate cell. Spatially averaged data obtained from this work showed higher mass-transfer values compared to those of previous work. This was as a result of the superior effect of the rectangular entry and exit configurations combined with the square-cut baffles over that of the three jets and small lozenge-shaped baffle openings used in the previous work. The square-cut baffles induced hydrodynamic phenomena such as flow reversal, wall impingement, and preferential flow effects, which all affected the mass-transfer distribution.

Plots of average mass transfer for different zones in the cell indicate rather similar behaviour to that found by other earlier workers. CFD modelling has confirmed the hydrodynamic basis for the areas of relatively high and low mass transfer. Strikingly similar behaviour in terms of mass-transfer behaviour has been indicated by comparison with naphthalene sublimation data of Japanese workers [11] for a similar system, but only consisting of two channels.

Acknowledgement

This work was performed under Brite-Euram III Contract No. BRPR-CT95-0008.

References

[1] F. Goodridge, G.M. Mamoor, R.E. Plimley, IChemE Symp. Ser. 98 (1985) 61.
[2] A.A. Wragg, A. Leontaritis, Chem. Eng. J. 66 (1997) 1.
[3] A.A. Wragg, D.J. Tagg, M.A. Patrick, J. Appl. Electrochem. 10 (1980) 43.
[4] C. Bengoa, A. Montillet, P. Legentilhomme, J. Legrand, J. Appl. Electrochem. 27 (1997) 1313.
[5] C.F. Oduoza, A.A. Wragg, J. Appl. Electrochem. 30 (2000) 1439.
[6] M.K. Chyu, J. Heat Transfer 113 (1991) 63.
[7] W.J. Yang, N. Zhang, J. Chiou, J. Heat Transfer 114 (1992) 354.
[8] S. Mochizuki, J. Takamura, S. Yamawaki, W.J. Yang, J. Turbomach. 116 (1994) 133.
[9] S. Dutta, J.C. Han, J. Heat Transfer 118 (1996) 578.
[10] T. Astarita, G. Cardone, G.M. Carlomagno, Heat Transfer in Turbulent Flows, ASME, HTD 318 (1995) 161.
[11] M. Hirota, H. Fujita, A. Syuhada, S. Araki, T. Yoshida, T. Tanaka, Int. J. Heat Mass Transfer 42 (1999) 1757.
[12] C.F. Oduoza, A.A. Wragg, Final Report of Brite-Euram III, Contract No. BRPR-CT95-0008, 1995–1998.
[13] N. Waterson, VKI, Brussels, Unpublished work included in [12].